YALE PEABODY MUSEUM

JOURNAL OF MARINE RESEARCH

The *Journal of Marine Research,* one of the oldest journals in American marine science, published important peer-reviewed original research on a broad array of topics in physical, biological, and chemical oceanography vital to the academic oceanographic community in the long and rich tradition of the Sears Foundation for Marine Research at Yale University.

An archive of all issues from 1937 to 2021 (Volume 1–79) are available through EliScholar, a digital platform for scholarly publishing provided by Yale University Library at https://elischolar.library.yale.edu/.

Requests for permission to clear rights for use of this content should be directed to the authors, their estates, or other representatives. The *Journal of Marine Research* has no contact information beyond the affiliations listed in the published articles. We ask that you provide attribution to the *Journal of Marine Research.*

Yale University provides access to these materials for educational and research purposes only. Copyright or other proprietary rights to content contained in this document may be held by individuals or entities other than, or in addition to, Yale University. You are solely responsible for determining the ownership of the copyright, and for obtaining permission for your intended use. Yale University makes no warranty that your distribution, reproduction, or other use of these materials will not infringe the rights of third parties.

Biological effects of Gulf Stream meandering

by Glenn R. Flierl[1] and Cabell S. Davis[2]

ABSTRACT

A modeling study was conducted to examine the effects of time-dependent mesoscale meandering of a jet on nutrient—phytoplankton—zooplankton (NPZ) dynamics. The jet was represented as a quasi-geostrophic flow using the method of contour dynamics. Two cases for biology were examined: 1) plankton in a mixed layer of fixed depth and 2) plankton at the base of a mixed layer (i.e., pycnocline) of variable depth. When the mixed layer depth is fixed, nutrient upwelling and dilution of the phytoplankton and zooplankton populations occur along the northward branch of the meander. The additional nutrients and reduced grazing pressure leads to significant enhancement (10–20%) of the phytoplankton production and biomass, while the zooplankton biomass decreases similarly. For plankton on a material surface of variable depth, phytoplankton growth in the pycnocline is increased by the higher light levels encountered during along-isopycnal upwelling. The nutrients decrease and the zooplankton mass in the pycnocline increases by a small amount downstream of the phytoplankton peak. Although the biological enhancements found are not large, the results suggest that vertical motions resulting from mesoscale oceanographic features such as jet meanders and mid-ocean eddies can be an important source of new nutrients for oceanic plankton production.

1. Introduction

Oceanic frontal regions have been widely observed as areas of enhanced productivity, biomass, and numerical abundance of planktonic organisms (Houghton and Marra, 1983; Olson and Backus, 1985; Gilham *et al.,* 1985; Lutjeharms *et al.,* 1985; Dengler, 1985; Richardson, 1985). Modeling studies indicate that such enhancement can be due to vertical migration interacting with physical convergence/divergence (e.g. Olson and Backus, 1985; Franks, 1992) or to enhancement of phytoplankton growth via nutrient upwelling into the mixed layer (Holligan, 1981; Seliger *et al.,* 1981; Houghton and Marra, 1983; Traganza *et al.,* 1987).

Upwelling induced by small eddies formed along the western edge of the Gulf Stream south of Cape Hatteras has been shown to cause enhanced production and biomass of phytoplankton in this area (Yoder *et al.,* 1981). Effects of mesoscale perturbations of the Gulf Stream and other western boundary currents on resident

1. Department of Earth Atmospheric and Planetary Sciences, M.I.T., Cambridge, Massachusetts, 02139, U.S.A.
2. Woods Hole Oceanographic Institution, Woods Hole, Massachusetts, 02543, U.S.A.

phytoplankton and zooplankton populations have not been studied. More generally, the effects of mesoscale frontal dynamics on basic nutrient—phytoplankton—zooplankton (NPZ) dynamics remain poorly understood.

As part of the BIOSYNOP program (an interdisciplinary study of Gulf Stream meanders, Olson, 1990), we have developed process oriented models to examine interactions between quasi-geostrophic flow fields and plankton dynamics. In the present paper we report results of an analytical and numerical study, based on the method of contour dynamics, which examines NPZ dynamics in a meandering mesoscale jet.

We develop a simple model to describe the effects of Gulf Stream meandering on the biological populations. The calculations are made with a 1½ layer quasigeostrophic contour dynamics model, a simple mixed layer model, and a three component biological system. We realize that many aspects of the model—both physical and biological—can be improved and made more complex. But we feel that examining the least complex version can illustrate the importance of the physical dynamics and the tendencies to be expected.

2. Mixed layer biology and physics

Since the biological dynamics of interest are mainly within the upper mixed layer, we need a simple representation of the mixed layer to combine with the deeper geostrophic flows. We begin with the equation for the evolution of a property B (such as the concentration of one of the biological variables) under the influence of advection, turbulent vertical mixing, and biological sources/sinks

$$\frac{\partial}{\partial t} B + \nabla \cdot (\mathbf{u}B) + \frac{\partial}{\partial z}(wB) = R(B, z) - \frac{\partial}{\partial z}\overline{(w'B')} \qquad (2.1).$$

where $\mathbf{u}$ is the horizontal mesoscale velocity, w the mesoscale vertical velocity. The turbulent fluctuations in vertical velocity and the biological property are given by w' and B' while the variables without primes represent the average values. The source/sink term, R, represents all the biological interactions which may alter the concentration. Note that some of these may be explicitly depth-dependent: uptake of nutrients, for example is a function of light intensity. We have not included horizontal transport by turbulence since we are building a model which in principle includes the mesoscale motions; the fluxes by the remaining sub-grid-scale motions have negligible influence during the time scales of interest. However, the contour dynamics model developed in Section 3 is not configured to resolve the small scale shingling and intrusions which can intermingle populations across the Stream. Such mixing would occur in a model with a much more detailed representation of the structure of the Stream; again, however, we expect the effects of such interchanges to be mainly important in influencing the long term average biological distributions.

Following the standard "bulk" mixed layer modeling procedure (c.f. Niiler, 1977)

we integrate (2.1) vertically from just below the mixed layer to the surface and assume that turbulent fluxes vanish at the top and bottom; we find

$$\frac{\partial}{\partial t}\int_{-h}^{0} B + \nabla \cdot \int_{-h}^{0} \mathbf{u}B - B^{-}\left(\frac{\partial}{\partial t}h + \mathbf{u}\cdot\nabla h + w(-h)\right) = \int_{-h}^{0} R$$

with h being the mixed layer depth and B^{-} being the value just below the mixed layer. If the mixing is sufficiently intense, B is uniform within the mixed layer and can be pulled outside the integrals. Using conservation of mass (consider $B = 1$, $R = 0$ in (2.1) and in the equation above)

$$\frac{\partial}{\partial t}h + \nabla \cdot \int_{-h}^{0} \mathbf{u} = \frac{\partial}{\partial t}h + \mathbf{u}\cdot\nabla h + w(-h)$$

and taking the horizontal velocities in the mixed layer to be uniform gives the result

$$\frac{\partial}{\partial t}B + \mathbf{u}\cdot\nabla B + (B - B^{-})\frac{1}{h}\left(\frac{\partial}{\partial t}h + \mathbf{u}\cdot\nabla h + w(-h)\right) = \frac{1}{h}\int_{-h}^{0} R$$

which can be written in terms of the entrainment velocity

$$w^* \equiv \frac{\partial}{\partial t}h + \mathbf{u}\cdot\nabla h + w(-h) \tag{2.2}$$

(the rate at which fluid crosses the moving mixed layer base) as

$$\frac{\partial}{\partial t}B + \mathbf{u}\cdot\nabla B + (B - B^{-})(w^*/h) = \frac{1}{h}\int_{-h}^{0} R. \tag{2.3}$$

When the mixed layer is entraining $w^* > 0$, the concentration of the property B is diluted (or increased if B^{-} is larger) by the flux of material from below (see Fig. 2.1); in contrast, when the mixed layer is detraining $w^* < 0$, the deeper properties match those in the mixed layer instantaneously so that there is no change in the mixed layer properties (except, of course, for the biological dynamics, R). We include this asymmetry between upwelling and downwelling by defining the dilution term

$$s = \frac{w^*}{h}\,\mathscr{H}\!\left(\frac{w^*}{h}\right) \tag{2.4}$$

with $\mathscr{H}$ being the step function (zero when its argument is negative—downwelling through the mixed layer base—and one when its argument is positive—upwelling across the base). In the case which shall be relevant below, the individual source—sink terms have fairly simple z dependence so that the vertical average can be evaluated explicitly. The coefficient for uptake of nutrients (see 3.2 below) then depends on the vertically averaged light level and thus becomes a function of h; as a result the interaction terms in (2.3) can be written as a function of the mixed layer
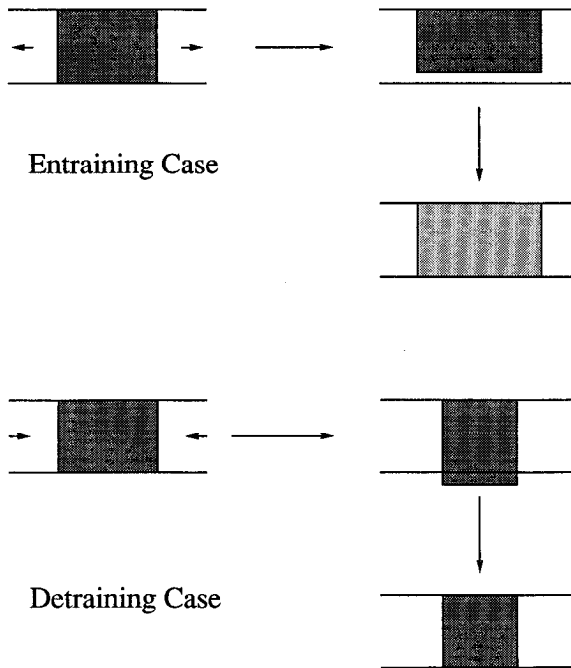
Figure 2.1. Entraining mixed layer, showing dilution. Detraining mixed layer showing no change in concentration.

biological quantities and the mixed layer depth. Thus our equation for the biological properties takes the form

$$\frac{\partial}{\partial t} B + \mathbf{u} \cdot \nabla B = -s(B - B^-) + R(B, h). \tag{2.5}$$

To close the mixed layer model, of course, we need some specification of the entrainment velocity w^*. Commonly, this would involve a temperature equation like (2.4) but including a heat flux at the upper boundary and a kinetic energy equation including input from the wind stress plus dissipation. Instead, we shall consider the two limits, a non-entraining layer ($w^* = 0$) and a mixed layer held at a fixed depth by wind stresses ($w^* = w$).

The physics enters the biological equation (2.5) in three ways: the horizontal flows advect the biota laterally, the vertical velocities (w) can move the base of the mixed layer so that h changes, or they can cause entrainment across the base (w^*). The two are, of course, related in the sense that a specification of the entrainment velocity gives one in terms of the other by (2.2). If we define

$$S = \frac{w}{h} \tag{2.6}$$

(which we refer to as the "stretching" term, though strictly speaking the rate of stretching is $-S$) we have

$$s = \left(\frac{D}{Dt}\ln h + S)\right)\mathscr{H}\left(\frac{D}{Dt}\ln h + S\right). \tag{2.7}$$

The two cases described above correspond to

$$\text{Non-entraining: } s = 0, \quad \frac{D}{Dt}\ln h = -S \tag{2.8}$$
$$\text{Fixed depth: } h = h_0, \quad s = S\mathscr{H}(S).$$

The non-entraining limit does not give a very large response, since the changes in average light level are rather small. Instead, we shall focus on a similar problem for particles on a "material surface" just below the mixed layer. In that case, we solve (2.5) with $s = 0$ but use the value of R at depth $h(t)$ rather than averaged over the mixed layer. This corresponds to the behavior expected for the ecosystem just below the mixed layer; the variability comes about because the plankton are lifted up into regions with different light levels. We expect a stronger response here, since the relative changes in light level are greater. In the second case, we examine the plankton dynamics within the mixed layer as it is affected by entrainment of water from below which has high levels of nutrient and low phytoplankton and zooplankton biomass.

3. Biological dynamics

Now we explicitly define the biological system to be considered. We shall use a conventional phytoplankton—zooplankton—nutrient model (e.g., Steele, 1977) and define $P = B_1$, $Z = B_2$, and $N = B_3$, all in nitrogen units. The total amount, $N_0 = \Sigma B_i = B$ is conserved along trajectories and we can therefore set $N = N_0 - P - Z$. For the biological interactions—the term $R(B, h)$ in (2.5)—we have used simple forms,

$$R_1 = u\bar{I}(h)\frac{PN}{k_s + N}bP - gPZ - bP$$
$$R_2 = agPZ - dZ \tag{3.1}$$
$$R_3 = -u\bar{I}(h)\frac{PN}{k_s + N} + bP + g(1 - a)PZ + dZ$$

with the terms representing uptake of nutrients, phytoplankton death, grazing, assimilation of grazed material, and zooplankton death (Fig. 3.1). In the nutrient equations, all losses are remineralized locally so that total nitrogen is conserved. The lack of vertical migration and the rapid remineralization of the zooplankton implies that they more closely represent microzooplanktonic consumers than larger crustacean grazers such as copepods or krill. While many other more complicated forms
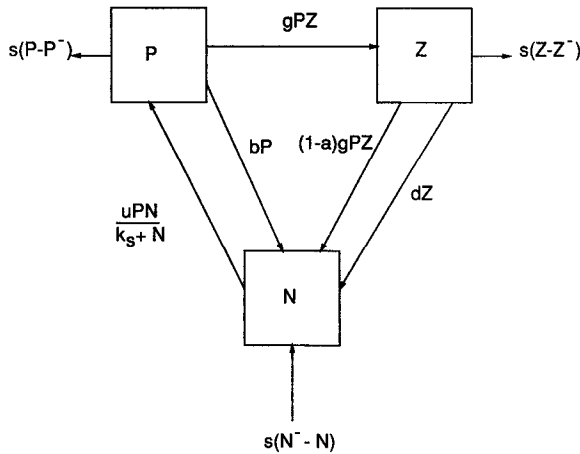
gPZ

s(P-P⁻)

P

Z

s(Z-Z⁻)

bP   (1-a)gPZ

dZ

$\frac{uPN}{k_s+ N}$

N

s(N⁻ - N)

Figure 3.1. Biological model. The exchanges between the phytoplankton, zooplankton, and nutrients represent grazing $[gPZ]$, nutrient uptake $[uPN/(k_s + N)]$, phytoplankton death $[bP]$, unassimilated/excreted material $[(1 - a)gPZ]$, and zooplankton death $[dZ]$. The upwelling, the terms proportional to s, lead to dilution of the phytoplankton and zooplankton, and to input of nutrients.

could be used (and we have also explored a model with the uptake term being a simple product of P and N, rather than the more common Michaelis-Menton form), the important qualitative behavior of the model is governed solely by the fact that there is a single stable equilibrium as discussed below. We examined an Ivlev grazing curve (Ivlev, 1955) and found that the response to periodic meandering is qualitatively similar. Other formulations such as Franks *et al.* (1986) could be used, but, given that the steady states are not very different (Wroblewski *et al.*, 1988), we do not anticipate any significant differences from (3.1). However, models with more complex biology, having multiple fixed points, some unstable, can exhibit complex and chaotic behavior (e.g. Steele and Henderson, 1992; Pascual, 1993), and it would be quite interesting to examine the effects of meandering on such a system. But in the absence of adequate information on the exact forms for the biology, we have chosen to use the simple approximations given above.

The light intensity will be assumed to fall off exponentially with a scale of 17 m and will be normalized so that $\bar{I}(50 \text{ m}) = 1$

$$I = \frac{\exp(-z/17)]}{(17/50)[1 - \exp(-50/17)]} . \tag{3.2}$$

For varying mixed layer depths, we have

$$\bar{I}(h) = \frac{(17/h)[1 - \exp(-h/17)]}{(17/50)[1 - \exp(-50/17)]} . \tag{3.3}$$

Parameter values for biology were chosen to approximate oligotrophic oceanic regions and were based on the following considerations (units will be days, μmol/l, and km, and the mixed layer depth h will be taken to be 50 m so that $\bar{I} = 1$). Deep nitrate concentration is 10 μmol/l, Lewis *et al.* (1986) and at equilibrium the total nitrogen is partitioned in the ratio $P{:}Z{:}N = 2{:}1{:}0.1$. Thus steady state values are $P = 6.452$, $Z = 3.226$, and $N = 0.323$. Zooplankton ingest 100% of their initial body weight in one day (e.g., Huntley and Boyd, 1984); thus if all this were assimilated, their biomass would double in one day and $gP = 0.7$. They assimilate 70% of the food they graze (Landry *et al.*, 1984) so $a = 0.7$; the equilibrium balance $R_2 = 0$ implies $d = 0.49$ so that half the zooplankton mass is lost to mortality and excretion per day. In saturating conditions ($N \rightarrow \infty$), phytoplankton grow at one doubling per day so that $u = 0.7$ and we take the equilibrium nitrate level to be twice the half-saturation value $k_s = N/2$. The equilibrium condition $R_1 = 0$ then gives $b = 0.117$ for the rate of loss of phytoplankton biomass by cell death.

Equilibria. We can gain insight into the biological behavior by considering the dynamics in the absence of physical forcing. (Note that the equilibria in this case will not generally be the same as the mean state with physical forcing because of entrainment/detrainment; c.f., Section 5a.) We have three possible steady states with $R_1 = R_2 = R_3 = 0$:

I: $P = 0$, $Z = 0$, $N = N_0$

II: $P = N_0 - bk_s/(u\bar{I} - b)$, $Z = 0$, $N = N_0 - P$

III: $P = d/ag$,   (3.4)

$\qquad gZ^2 + [b - u\bar{I} - g(k_s + N_0 - P)]Z + u\bar{I}(N_0 - P) - b(k_s + N_0 - P) = 0$,

$\qquad N = N_0 - P - Z$

(with the negative root used in the solution of the quadratic). As the mixed layer depth is increased, we switch from the third solution to the second (at $h = 208$ m for the parameters above) and to the first (at $h = 214$ m) as successive trophic levels are no longer able to sustain themselves.

The equilibrium defined above (particularly III) will be used as initial conditions in the various models. It is important to note that we will not discuss the variations in total nitrogen N_0 (and therefore P, Z, and N) which might occur across the jet. In essence, we are focusing on the variations of properties on a single material line corresponding to the jet axis. We could reconstruct a spatial picture of the concentrations by considering a whole set of material lines spanning the Stream; at that point, we could include variations in N_0 from line to line. In the Eulerian picture, we would then see spatial variability associated with translation of the different lines as well as that associated with the vertical movements (which is the focus of the present work). This viewpoint emphasizes one of the difficulties in detailed comparison of our

model to oceanic data: if there are large cross-stream variations in properties, it is hard to separate biological variability on a material line from apparent variations caused by errors in determining the position of a material line.

4. Interior physics and biology

a. Physics. We shall use a quasigeostrophic layer model to represent the physical dynamics of the meandering jet. The Rossby number of the Gulf Stream, of course, is not very small, and therefore we expect the behavior will show some differences from the QG system. Nevertheless, this model provides the simplest representation of the velocity fields and does seem to give reasonable patterns for not only u and v, but also the vertical velocity w. The β effect will be neglected since the flows are very strong.

We shall assume that the velocity in the mixed layer is that of the geostrophic flow beneath it, and neglect wind-driven/inertial motions. For calculating advections, this is a good approximation, since the flows in the jet are quite strong compared to any wind-driven surface layer flow and the inertial circles are small compared to particle displacements associated with the jet motions. However, we cannot be so sure that the vertical velocities, associated with the horizontal divergence of the flow, are dominated by the deep upwelling and downwelling related to the meandering. Below, we shall see that the Ekman pumping is usually smaller than the meander-driven vertical flows. And we might also expect that pumping would have quite different space and time scales and the biological variability produced by it would not be correlated with the meanders, unlike the part of the variability we are investigating.

While we could use a full multi-layer model, we shall, for simplicity, specialize to the 1½ layer model of Pratt and Stern (1986). Meacham (1991) has demonstrated that a two layer model does have rather different dispersion relationships from a 1½ layer model; Flierl and Meacham (1993) discuss this more fully and demonstrate that for reasonable depth ratios, there is a strong instability in the wavelength band of interest. However, they also show that the nonlinearity can stabilize the wave; thus it is reasonable to consider a steadily propagating wave problem and to concern ourselves primarily with the upper layer.

For the 1½ layer model, the dynamically important quantity is the potential vorticity q which is related to the stream function ψ by

$$q = \nabla^2\psi - \gamma^2\psi$$

with $1/\gamma$ being the deformation radius, the characteristic horizontal scale for surface intensified mesoscale flows (c.f., Pedlosky, 1987). The potential vorticity is conserved in the motion

$$\frac{D}{Dt}q = \frac{\partial}{\partial t}q + \mathbf{u} \cdot \nabla q = 0.$$

First let us consider the stretching associated with the vertical motions. We assume that the mixed layer is always contained within the top layer in which the stretching is depth-independent; in that case the meander-induced stretching can be determined from the vorticity equation:

$$S = \frac{w}{h} = -\frac{1}{f}\left(\frac{\partial}{\partial t} + \mathbf{u} \cdot \nabla\right)\nabla^2\psi = -\frac{1}{f}\frac{D}{Dt}\nabla^2\psi.$$

Invoking conservation of potential vorticity gives

$$S = \frac{\gamma^2}{f}\frac{D}{Dt}\psi = -\frac{\gamma^2}{f}\frac{\partial}{\partial t}\psi \tag{4.1}$$

in the 1½ layer case.

To calculate the depth of a material surface, we can integrate

$$\frac{D}{Dt}\ln h = -S = \frac{\gamma^2}{f}\frac{D}{Dt}\psi$$

so that

$$\ln\left(h/h_0\right) = \frac{\gamma^2}{f}(\psi - \psi_0). \tag{4.2}$$

We have calculated the flow fields using a contour dynamical model (c.f. Pratt and Stern, 1986; Meacham, 1991); the potential vorticity is assumed to be piecewise constant to the north and to the south of the jet (see Fig. 4.1a)

$$(\nabla^2 - \gamma^2)\psi = -\gamma U_0 + 2\gamma U_0 \mathcal{H}(y - \eta). \tag{4.3}$$

Here U_0 is the peak velocity of the undisturbed jet. The interface separating the high and low potential vorticity fluid, is located at $y = \eta(x, t)$. Lagrangian points on this potential vorticity contour move according to

$$\frac{dx}{dt} = u(x, \eta, t) = -\frac{\partial}{\partial y}\psi(x, \eta, t)$$
$$\frac{dy}{dt} = v(x, \eta, t) = \frac{\partial}{\partial x}\psi(x, \eta, t). \tag{4.4}$$

We can represent the velocities of points on the contour as integrals of functions over the contour and thereby derive a closed system predicting the evolution of the contour as a functional of the contour. In particular, if we differentiate (4.3) with respect to x, we find

$$(\nabla^2 - \gamma^2)v = -2\gamma U_0\delta(y - \eta)\frac{\partial}{\partial x}\eta$$
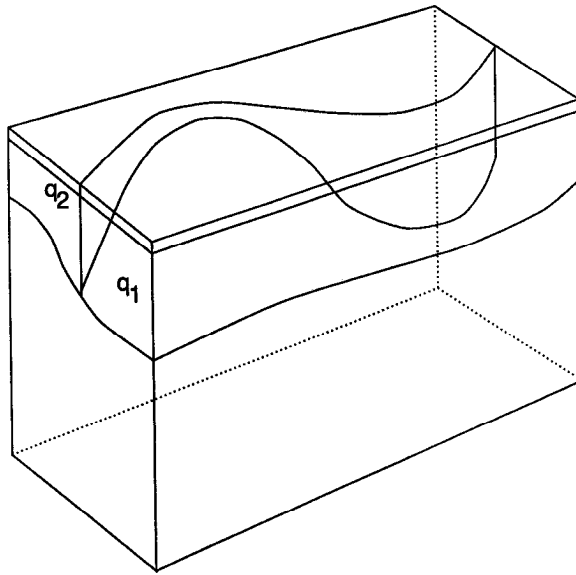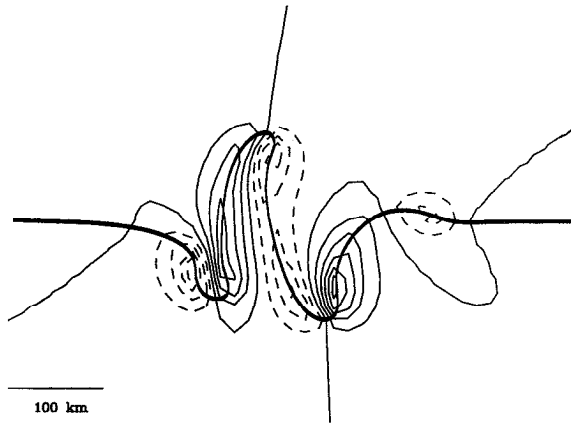
Figure 4.1. (a) Sketch of model geometry, showing potential vorticity front, thermocline shape, and mixed layer, (b) Vertical velocity pattern. The thicker line shows the axis position. The contours are of S in intervals of $0.05/d$ (negative are dashed). For a mixed layer of 50 m depth, these contours represent vertical motions at the base of the mixed layer with contour intervals of 0.003 cm/sec (peaking at about 0.015 cm/sec). For the thermocline the velocities are a factor of 10 larger, (c) Streamfunction and potential vorticity contour. The streamfunction contours also show the depth of a material surface; the tendency for northward traveling particles to shoal (decreasing depth) and southward going parcels to deepen can be seen in the way that the axis crosses the streamlines. (d) Material surface depth as a function of distance along the contour derived by assuming the propagation is steady, c.f. Eq. (4.9), and with ψ from the previous figure. The dashed lines show the northward displacement (in km) divided by 10.
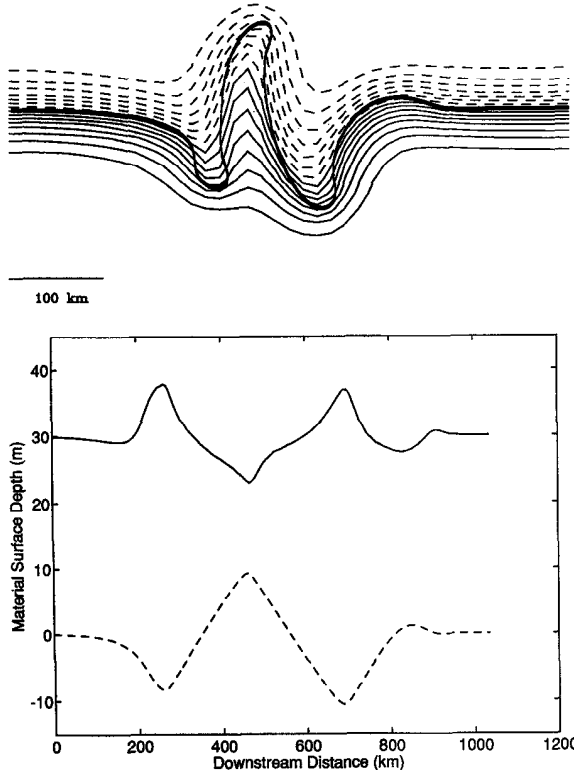
Contours of ψ

100 km

Figure 4.1. (Continued)

which can be solved using a Green's function

$$v(x, y, t) = -2\gamma U_0 \int dx' \int dy' G(x, y | x', y') \delta(y' - \eta(x', t)) \frac{\partial}{\partial x} \eta(x', t)$$

$$= -2\gamma U_0 \int dx' G(x, y | x', \eta(x', t)) \frac{\partial}{\partial x} \eta(x', t)$$

$$= -2\gamma U_0 \int d\eta\, G(x, y | x', \eta(x', t))$$

where the last integral is a contour integral along the interface. The Green's function satisfies the equation

$$(\nabla^2 - \gamma^2) G(x, y | x', y') = \delta(x - x') \delta(y - y')$$

and gives the disturbance in the streamfunction field produced at a point (x, y) by a point vortex at position (x', y'). It is given in terms of the modified Bessel function by

$$G = -\frac{1}{2\pi} K_0(\gamma\sqrt{(x - x')^2 + (y - y')^2}).$$

A y derivative of (4.3) leads to a similar equation for the zonal velocity; together, we have

$$
\begin{aligned}
u &= -2\gamma U_0 \int dx' G(x, y | x', \eta(x')) \\
v &= -2\gamma U_0 \int d\eta G(x, y | x', \eta(x'))
\end{aligned}
\tag{4.5}
$$

with the integrals taken along the interface contour. As Pratt and Stern (1986) comment, one does need to be careful if one is working in an unbounded domain to get the proper limit of the zonal velocity as $\eta \to 0$. These are the basic equations expressing the velocities as a functional of the contour and can be used to calculate the movement of the points on the contour according to (4.4).

When the mixed layer depth is fixed, the entrainment term is given by

$$s = S\mathscr{H}(S).$$

For the prediction of the vertical velocities, we need the time change of the streamfunction in order to complete (4.1). This can be calculated by differentiating (4.3)

$$
\begin{aligned}
\frac{\partial}{\partial t} \psi &= -2\gamma U_0 \int dx' G(x, y | x', \eta) \frac{\partial}{\partial t} \eta \\
&= -2\gamma U_0 \int [dx' v(x', \eta) - d\eta u(x', \eta)] G(x, y | x', \eta).
\end{aligned}
\tag{4.6}
$$

Thus the vertical stretching term S can be computed solely in terms of contour integrals. Figure 4.1b shows the vertical velocity pattern in a typical wave. The depth of a material surface can also be written in terms of contour integrals; however, the form is complex and will not be used below.

In summary, the time-dependent evolution of the contour can be found by calculating the velocity on each point on the contour, using the Greens function integral (4.5) over the contour itself. These velocities are used to advance the points on the contour, using an ODE algorithm such as Runge-Kutta. Meacham (1991) has a detailed discussion of the procedure and the differences between the equivalent barotropic model and two layer models. The stretching term can be evaluated at all points where the biological variables are required using (4.6) and the Lagrangian motion of those points can be computed with (4.4). Finally, we need to specify the evolution of the mixed layer depth in order to calculate s and $R(B, h)$ in (2.4).

If we now consider steadily propagating wave patterns, we can replace the time

derivative by a space derivative so that

$$S = c\,\frac{\gamma^2}{f}\,\frac{\partial}{\partial x}\,\psi = c\,\frac{\gamma^2}{f}\,v \tag{4.7}$$

with v calculated by the ordinary contour dynamical algorithm. On the contour itself, the centerline of the jet, we can find an alternate expression for the vertical velocity:

$$S = \frac{c\gamma^2}{f}\,\frac{D}{Dt}\,\eta. \tag{4.8}$$

The vertical motions can be understood very simply: in the case of steadily propagating patterns, particles move along a potential vorticity contour, so that $\psi + cy$ is constant following a particle. As the fluid moves north, ψ and thus the depth must decrease. Upwelling occurs as the particles move north and downwelling happens on the southward branch as observed by Bower and Rossby (1989). The same effect is seen in unsteady situations as shown in Figure 4.1c, where we have superimposed the streamfunction field (proportional to the depth of a material surface) on the potential vorticity contour. This view of the upwelling is essentially the same as that discussed by Bower (1991); however, we have used a flow pattern which is a solution to the dynamical equations (4.5–6).

For the steadily propagating case, the variations in the depth of a material surface for the fluid parcels on the contour are also simple:

$$\ln\,(h/h_0) = \frac{\gamma^2}{f}\,\psi = -c\,\frac{\gamma^2}{f}\,\eta \tag{4.9}$$

so that the surface is shallow when the jet meanders to the north and deep when it moves south as shown in Figure 4.1d. The biological changes induced by steadily propagating, periodic meanders will be discussed in Section 5.

b. Biology. Since plankton in the mixed layer are affected by mixing across the base of the layer, we need to describe the biological dynamics beneath the mixed layer. We can calculate the equilibrium distribution assuming the plankton in the mixed layer see the depth-averaged level of light, while those below see the local light levels. In effect, we have an $\bar{I}$ given by (3.3) within the mixed layer $(-h < z < 0)$ and by (3.2) for the deeper fluid. The curves for effective light intensity for two cases, $h = 30$ m and $h = 50$ m are shown in Figure 4.2a, and the equilibrium distributions are plotted in Figure 4.2b and 4.2c. For the case of $h = 30$ m, the phytoplankton are grazer-controlled even below the mixed layer and thus maintain a constant concentration (solution III). But there is a decrease in zooplankton and an increase in nutrients across the base of the mixed layer. Deeper, the zooplankton die out and the phytoplankton begin to decrease in concentration being light-limited (solution II).
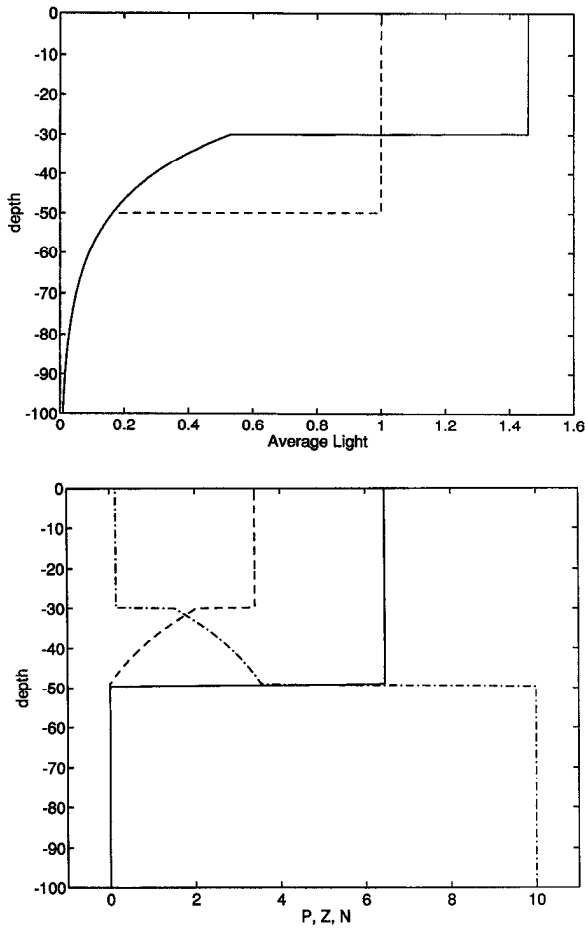
Figure 4.2. (a) Light levels for the 30 m and 50 m mixed layer depths, (b) and (c). Equilibrium distributions of P (solid), Z (long dash), and N (dash-dot) for the 30 m and 50 m mixed layer depths.

Finally, below a critical depth, there are only dissolved nutrients (solution I). When the mixed layer is deeper, phytoplankton and zooplankton cannot survive beneath the base of the mixed layer because the light levels are too low. Thus we have two different scenarios for P^- and Z^-: when the mixed layer is 50 m, the deep values are 0, while the shallower case gives $P^- = 6.452$, $Z^- = 2.024$ in contrast to the mixed layer value of $Z = 3.402$ in this situation with higher average light levels.

In either case, we assume that any particles descending below the mixed layer come back to equilibrium before returning to the mixed layer. This assumption is valid if the time scale for biological adjustment is short relative to the physical time scales; this is not necessarily the case, since the growth rates in the deep water tend to be quite slow because of the low light levels.
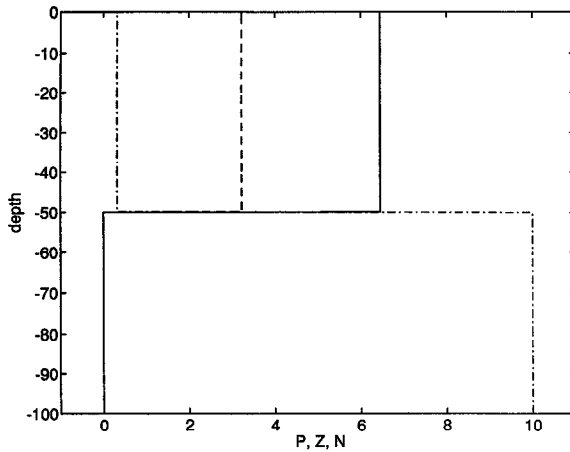
Figure 4.2. (Continued)

Including the processes described above gives two equations for the biological model:

$$\frac{D}{Dt} P = u\bar{I}(h) \frac{P(N_0 - P - Z)}{k_s + N_0 - P - Z} - bP - gPZ - s(P - P^-) \tag{4.10}$$

$$\frac{D}{Dt} Z = aPZ - dZ - s(Z - Z^-). \tag{4.11}$$

These equations, together with the physical equations (4.4–5) for particle motions, (4.6) for the stretching, (4.2) for the depth of a material surface, and an entrainment parameterization (c.f. Eq. 2.8), complete the specification of the model.

5. Spatially periodic meanders

a. Averages. If the forcing term s is periodic (following a particle down stream), then we can assume that P and Z are likewise periodic. We consider the case when the mixed layer depth is 50 m. If we divide (4.11) by Z and integrate over a Lagrangian period (i.e., the period following the particle), we find

$$\bar{P} = \frac{d + \bar{s}}{a} \tag{5.1}$$

showing that the average phytoplankton level is raised in the presence of periodic entrainment and detrainment. Note that, because the phytoplankton are grazer-controlled and the zooplankton equation is linear in P and in Z, it is only the entrainment across the base of the mixed layer which affects the average phytoplankton biomass. Essentially, the dilution of the zooplankton by entrainment of deeper water acts like an increase in the death rate; therefore, the average grazing pressure
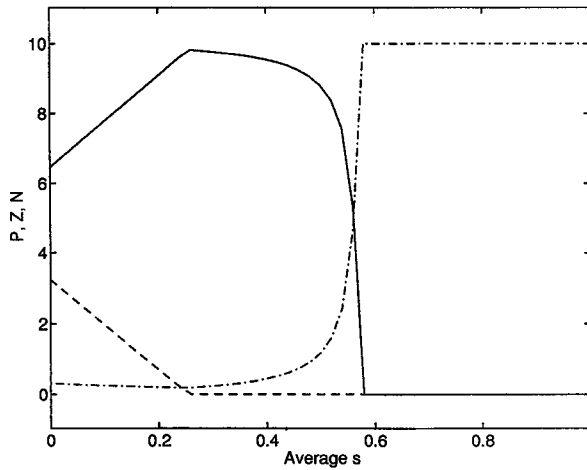
Figure 5.1. Average levels of the biological fields as a function of averaged upward motion.

is reduced. If the mixed layer is not changing in thickness so that $I(h) = 1$, we can similarly find the average zooplankton level by replacing b with $b + \bar{s}$ in (3.4) (effectively increasing the loss rate for phytoplankton). The average zooplankton level is reduced. Similar states corresponding to solutions I and II also exist. Figure 5.1 shows the variation of $\overline{P}$ and $\overline{Z}$ with upwelling $\bar{s}$. The upwelling dilutes the zooplankton; for the phytoplankton, however, the added nutrient and decreased grazing more than offsets the dilution by introduction of phytoplankton-free water from below. Other biological formulations (within the constraints of a single stable equilibrium) will show different sensitivities here; for example, an Ivlev grazing curve gives a stronger increase (decrease) in average phytoplankton (zooplankton) levels as the upwelling amplitude increases.

b. Linearization. We can linearize the physical dynamics to estimate the propagation rate for periodic meanders. The potential vorticity—streamfunction relationship (4.3) can be solved by Fourier expansion; the first terms are

$$\psi \simeq \frac{U_0}{\gamma} \begin{cases} 1 - e^{\gamma y} + A_-\eta e^{\sqrt{k^2+\gamma^2}\, y} & y < 0 \\ -1 + e^{-\gamma y} + A_+\eta e^{-\sqrt{k^2+\gamma^2}\, y} & y > 0 \end{cases}$$

where we assume that the axis displacement has the form $\eta = \eta_0 \sin (kx - kct)$. Matching ψ and $\Delta\psi$ at the position $y = \eta$ gives $A_- = A_+ = \gamma^2/\sqrt{k^2 + \gamma^2}$. From this formula, we find the streamfunction along the axis

$$\psi(x, \eta) = -U_0\eta + \frac{U_0}{\gamma}A_+\eta$$

$$= -U_0\eta\left(1 - \frac{\gamma}{\sqrt{k^2 + \gamma^2}}\right).$$

Requiring $\psi(x, \eta) + c\eta$ be constant leads to Pratt and Stern's dispersion relationship

$$c = U_0\left(1 - \frac{\gamma}{\sqrt{k^2 + \gamma^2}}\right) \tag{5.2}$$

as shown in Figure 5.2a.

To determine whether the upwelling is significant in the biological dynamics, we need an estimate of changes in depth of a material surface h/h_0 to see how light levels can change and an estimate of S in units of inverse days to compare with the biological time scales above. We assume that the deformation radius is 30 km, $f = 8.6/d$ and the centerline jet velocity is 1.5 m/s. Suppose we have a meander with peak to trough amplitude of 225 km, propagating at 10 km/d [corresponding to a 450 km wavelength using (5.2)]. A material surface at 30 m nominal depth will then range in depth from 25.9 m at the crest of the meander to 34.7 m at the trough (from 4.9). For light falling off exponentially with a 17 m e-folding scale, the light intensity on that material surface varies by about ±25%. On the other hand the light level averaged over the mixed layer varies by a much smaller amount, 9%, for the same excursion of a mixed layer nominally at 30 m depth. The angle of the axis is somewhat larger than 45° so that the northward velocity can reach 110 km/d; thus, we estimate from (4.7) that the maximum S is about 0.2/d. The full linear model gives a somewhat larger value, $S = 0.24$. Thus the upwelling can be expected to make a nontrivial contribution to the biological dynamics. An estimate of S directly from Gulf Stream data can be made from the information in Bower and Rossby (1989) or Bower (1989); dividing her peak vertical velocity of 0.18 cm/sec (0.16 km/d) by the mean depth of 0.6 km gives a similar value of $S = 0.26/d$.

For future reference, note that a stretching term $S \sim 0.3/d$ corresponds to vertical velocities of 0.21 cm/sec at the thermocline and 0.02 cm/sec at the base of the mixed layer. These are substantial; the mean Ekman pumping, for comparison, is about 2×10^{-4} cm/sec (Leetma and Bunker, 1978) while it may reach 0.1 cm/sec in a hurricane (Price, 1981). Thus the vertical motions are comparable to those which might arise from storms, but the time scales are considerably longer and, in contrast to wind-driven pumping, the vertical motion we consider is correlated with the meander excursions.

In the linearized theory, the amplitudes are arbitrary; we have chosen to make the peak-to-trough displacement of the axis equal to one half the meander wavelength. This is within the range where Pratt's model would suggest that the linear estimate of c is reasonable. With these choices we find the peak value of s (Fig. 5.2b) can be as large as 0.85/d for a wavelength of 110 km (which is really below the range where we might expect the QG 1½ layer model to be very accurate) to values of about 0.2/d–0.5/d in the range of wavelengths commonly observed. The excursion of a material surface (Fig. 5.2c) peaks at about 14 m but varies by only 5 to 10 m for reasonable wavelengths. For short scales, the depth excursion decreases because the
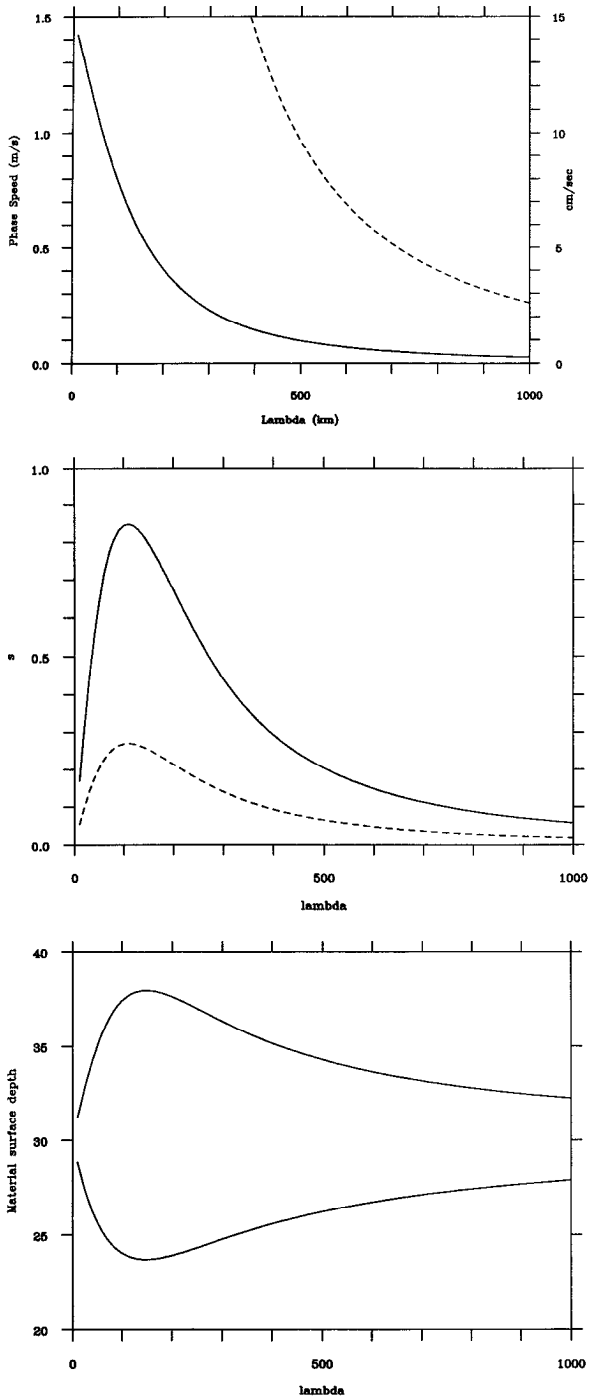
Figure 5.2. (a) Dispersion relationship (dashed lines correspond to right-hand scale), (b) Peak values and average values of s (in $1/d$) as a function of wavelength for the case of a fixed mixed layer depth of 50 m, (c) Minimum and maximum depth of a material surface nominally at 30 m depth.

meander amplitude decreases. The stretching term also decreases because $U_0 - c$ goes to zero. (Of course the QG simple front model is suspect at the shorter scales.) At the longer scales, the signals decay because the phase speed (responsible for the mismatch between the PV contour and the thermocline depth contours) decreases.

c. *Examples.* The biological equations were solved with a Runge-Kutta algorithm, beginning with the equilibrium values far upstream of the segment shown. Each figure gives the P, Z, N values versus the downstream distance.

For plankton in a 50 m mixed layer (Figs. 5.3a–d), at longer meander wavelengths, the disturbances are weak, because the motion of the wave is very slow. Essentially, c is proportional to k^2 while the amplitude of v is only proportional to $1/k$ (given the assumption that the amplitude is one fourth the wavelength). By (4.7), then, the stretching is weak. The phytoplankton peak somewhat upstream of the crest, while the zooplankton are lowest there. In a quasiequilibrium state (a very long wave), one would expect the extrema would occur where S is largest, half way between the trough and the crest; clearly the advection is still playing a role.

As the wavelength decreases to 500 km (Fig. 5.3b), the perturbations in all fields become stronger, while the phytoplankton average level increases and the zooplankton average level decreases. At even shorter wavelengths the dilution is strong enough that the zooplankton play a very minor role (c.f., the case with 200 km wavelength, Fig. 5.3c) and the model behaves like a $P - N$ model. Finally, at wavelengths near 100 km (Fig. 5.3d), the zooplankton are unable to survive; however, the die-out occurs rather slowly with substantial levels still existing 1000 km downstream. In the far downstream region shown in (5.3d), only phytoplankton and nutrients are found.

The linear model, with the aforementioned amplitude assumption, has been solved for a large range of wavelengths in order to determine the biological variability as a function of the meander wavelength. The amplitude of the stretching term (which can cause entrainment or detrainment) and the maximum vertical excursion of the material surface (nominally at 30 m) both peak at rather short wavelengths (Figs. 5.2b, c). The biological variation (Fig. 5.4a) also peaks at the shorter scales but remains sizable even at the scales of several hundred kilometers typical for meanders of the Gulf Stream. Note that at the short wavelengths, the average upwelling is strong enough so that the zooplankton cannot survive.

When the values below the mixed layer are taken from (3.2, 3.4) for the 30 m thick layer, the results are quite different; the variability is greatly reduced and is not very sensitive to wavelength (Fig. 5.4b). The jump in properties across the mixed layer base is simply too small for the entrainment to greatly influence the biology.

Finally, if we look at the material surface just beneath the base of a 30 m mixed layer (Fig. 5.5a), we see that the response is almost entirely in the phytoplankton and nutrient fields. The light levels cause increases and decreases in uptake rates; the
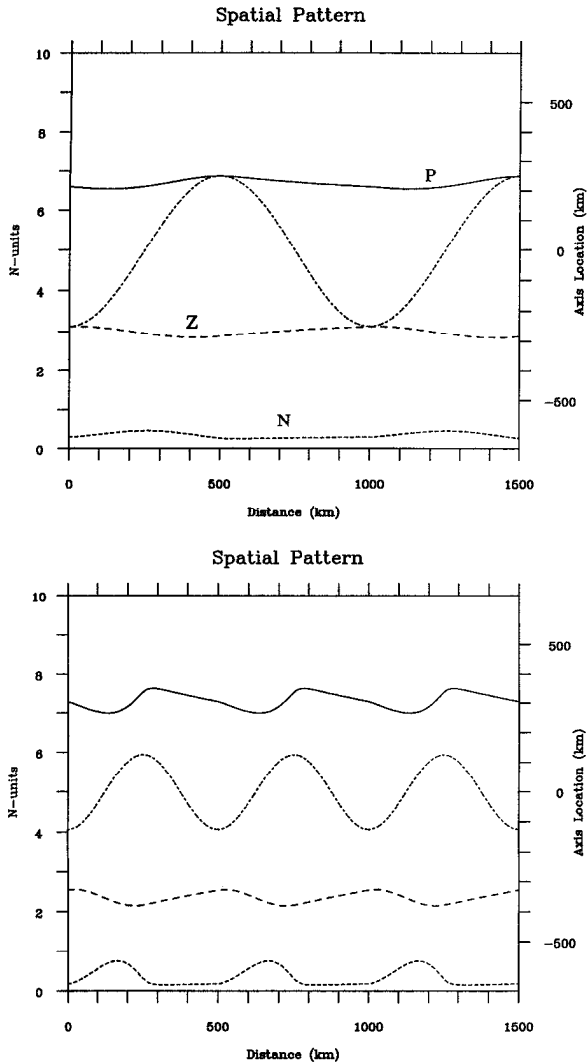
Spatial Pattern

Spatial Pattern

Figure 5.3. Phytoplankton (solid), zooplankton (long dash), and nutrient (short dash) distributions in a periodic wave. The axis position is also shown. Wavelengths of 1000, 500, 200, and 100 km are shown.

grazing and death rates stay fairly constant, so that the changes in uptake translate directly into increases or decreases in the phytoplankton. However, the changes are still small enough that the variations in zooplankton growth are weak. The nutrient field changes in the opposite sense to the phytoplankton. The variability is less sensitive to wavelength in the material surface case (Fig. 5.5b); essentially, the longer waves have larger north-south excursions, but, because they move more slowly, the

Spatial Pattern

Spatial Pattern
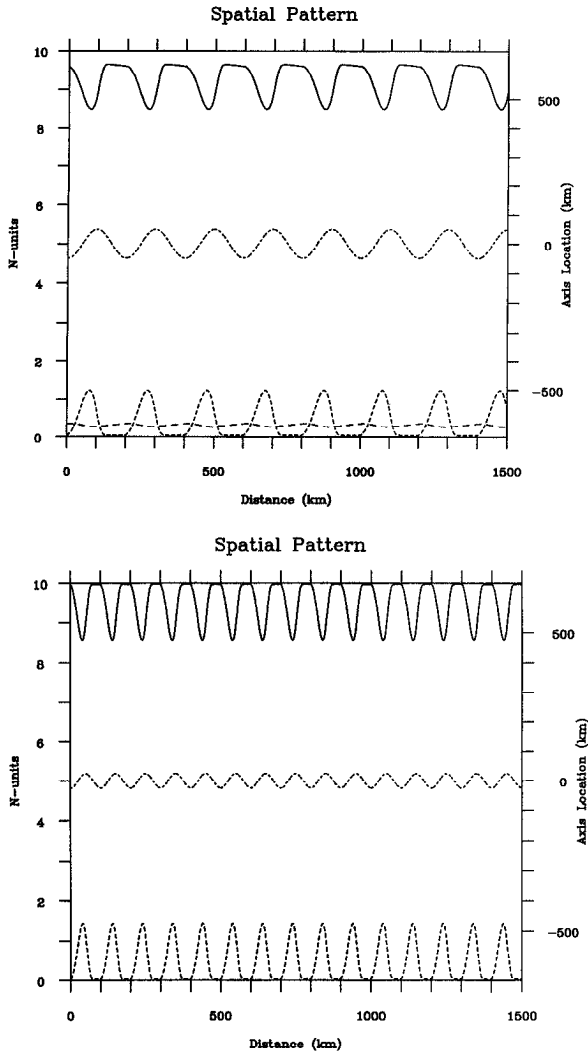
Figure 5.3. (Continued)

streamlines (or depth contours) and the PV contour are nearly aligned and the changes in height are not large.

6. Isolated disturbance

Next we show two examples of biological response to isolated meanders. First, we examine the equilibrium distribution of plankton assuming that the meander is propagating steadily without change of shape. Second, we show an example of time-dependent meander development using the case studied by Pratt and Stern
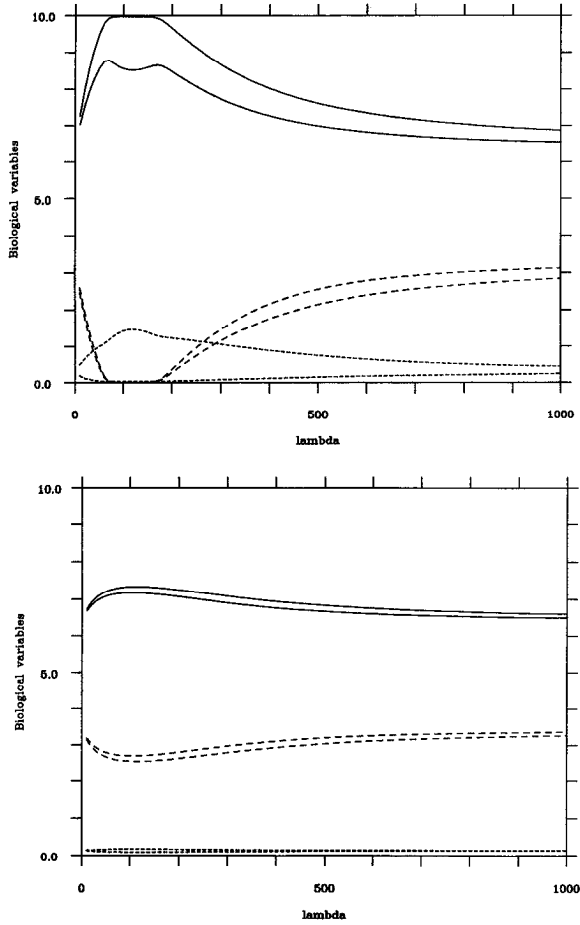
Figure 5.4. (a) The maximum and minimum values of P, Z, and N for waves of different wavelengths. Mixed layer depth is 50 m; (b) As above but with mixed layer depth 30 m.

(1986). In this case, the fully nonlinear equations for both the physical (4.4–6) and biological dynamics (4.10–11) are solved.

In the steady case, we construct a meander from a single cycle of a cosine wave and assume that it moves steadily with the phase speed predicted by the linear theory for an infinite wave train. This is, of course, not correct for either the linear theory or the nonlinear model. But it does give some idea of the impact of such a meander on the biology. We take the case of the 50 m mixed layer and a 500 km wavelength (Fig. 6.1). As the flow begins to move northward into the meander, upwelling causes dilution of the phytoplankton and zooplankton, while injecting nutrients into the mixed layer. The phytoplankton then increases in response to the enhanced nutrients and decreased grazing. They reach high levels at the eastern side of the crest, reducing
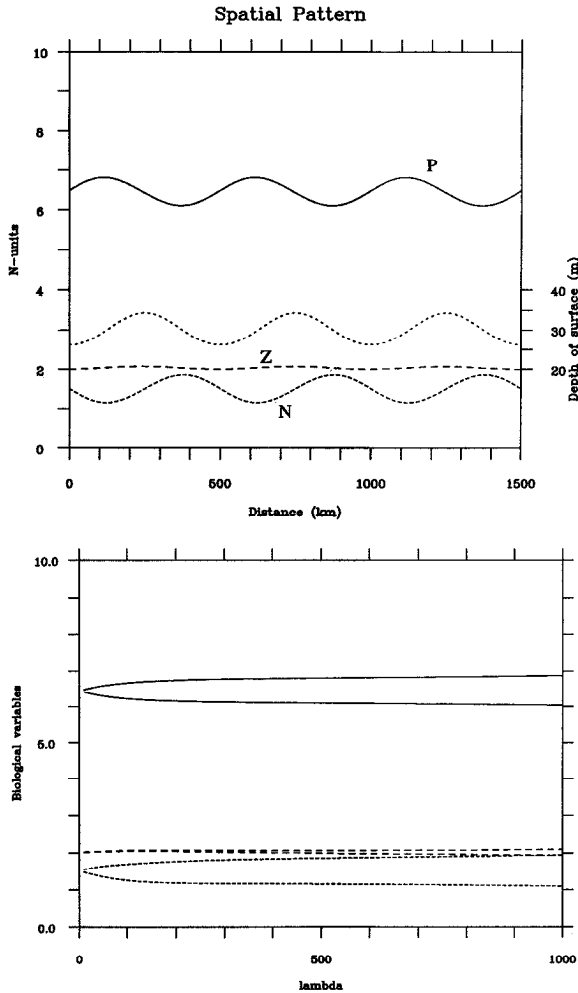
Spatial Pattern

Figure 5.5. (a) Phytoplankton, zooplankton, and nutrients for parcels on a material surface nominally at 30 m in a periodic wave with a 500 km wavelength. The depth of the surface is also shown; (b) Ranges of variables as in (5.4) but for the case of a material surface nominally at 30 m.

the nutrients to values lower than equilibrium; downstream, the zooplankton gradually recover and graze the phytoplankton back down.

In the time-dependent case, a three lobed meander develops into a ring during a time of about 4 days. Figure 6.2 shows the stretching occurring during this development; note the strong activity in the vicinity of the pinch-off region. The peak value of S is about 0.3/d ($w \sim 0.2$ cm/sec). There is generally still upwelling as the fluid approaches a crest and downwelling approaching a trough (refer back to Fig. 4.1b which shows the vertical velocity one day into the evolution).

Spatial Pattern
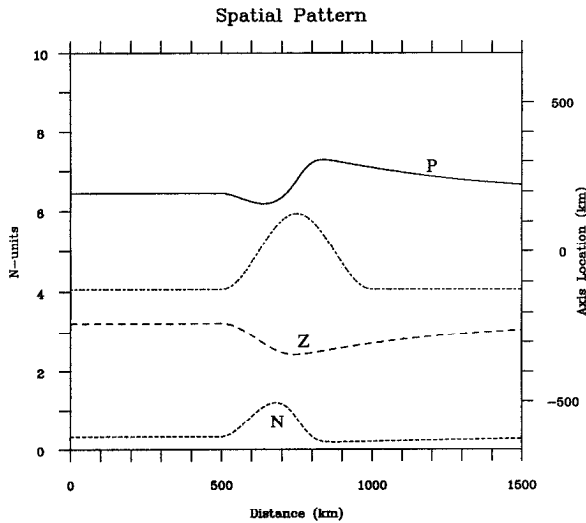
Figure 6.1. Effect of a single propagating bump of scale 300 km.

The biological fields (Fig. 6.3) show a response influenced by both the forcing and the advection. We show only the strongest case, with the 50 m mixed layer. The phytoplankton shows a slight decrease at the beginning of the meander because of dilution, before becoming strongly enhanced by the increased nutrient and the reduced grazing pressure. The zooplankton are diluted and cannot respond effectively to the enhanced phytoplankton (much as in the case of the changes in the

S on contour
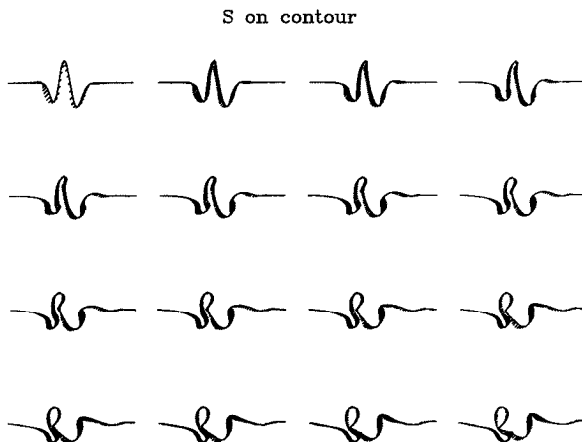
Figure 6.2. Development of a ring. The successive panels (left to right in each row) show the axis position, while the diagonal lines show *S* with northeast lines being positive and southwest negative. The frames are 20 deformation radii (600 km) in width. The time interval is ¼ day. Note the upwelling along the branches where fluid is flowing north, with the most intense motion in the region where pinch-off is occurring. See also Figure 6.3c.
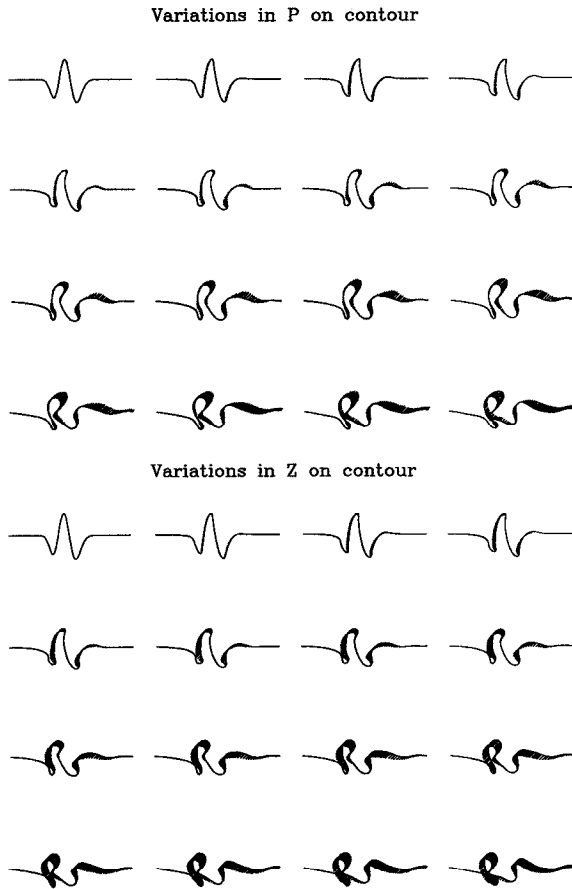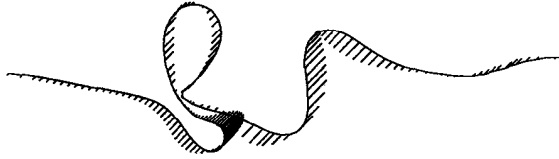
Variations in P on contour

Variations in Z on contour

Figure 6.3. (a, b) Associated perturbations of *P* and *Z* from their equilibrium values. (c, d, e). Pictures after 3.75 days. For magnitudes, see Figure 6.4.

average values for periodic meanders). These fields are carried into the eastern side of the meander by the advection; thus when a warm eddy is formed, the potential vorticity contour forming the edge of the ring is nearly everywhere high in phytoplankton and low in zooplankton.

We can examine the balances of terms in the individual biological equations as functions of along-axis distance, as shown in Figure 6.4. For the phytoplankton, the uptake of nutrients can increase by as much as 36%, while the grazing can decrease by 31%. As the nutrient balance shows, the input from recycling can decrease by about 22% in the regions with low zooplankton, but the dominant source of nutrient variability is in the upwelling of new nutrients. In the regions of strongest upwelling, this source is nearly equal to the rate of input from recycling. The dilution of phytoplankton can also significantly reduce the final growth rate. For the zooplank-

S on contour

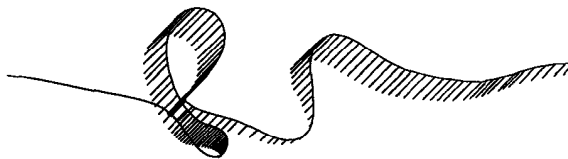Variations in P on contour
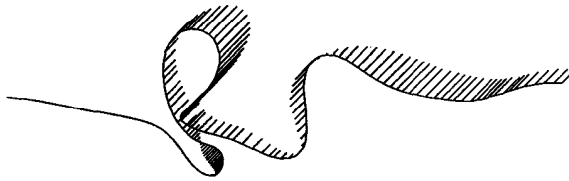
Variations in Z on contour

Figure 6.3. (Continued)

ton, the growth rate from assimilation varies by about 12% because of the phytoplankton fluctuations. The dilution is now a very significant mechanism for loss.

The case of cold eddy formation (which for the QG system can be obtained by simply changing the sign of the initial displacement) shows a somewhat different pattern of biological development. The vertical motion is reversed. Once again, the phytoplankton respond to the upwelled nutrients and reach higher levels at the
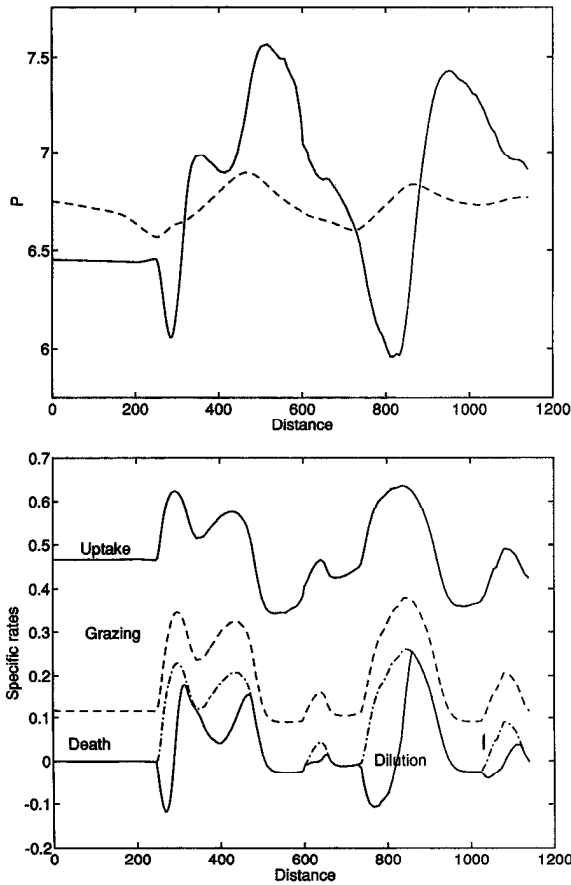
Figure 6.4. (a) Balances of terms in the phytoplankton equation, showing how the uptake is partitioned into grazing, death, and dilution (leaving DP/Dt). Dashed line shows the latitude as a function of downstream distance. (b) Tendencies to increase N associated with recycled nutrients (dash-dot), upwelling of nutrient-rich water (dash), and their ratio (solid). (c) Zooplankton balances.

meander crests and just beyond, with the zooplankton decreasing by dilution. Now, however, the flow moves these areas down into the western side of the developing cold ring, so that the phytoplankton are enhanced in the pinch-off region and along the downstream part of the meander, but not over the entire ring. In the eastern side, there is upwelling, but it is mainly diluting the fields; the response to the increased nutrient occurs downstream. In contrast, the upwelling on the western side of a developing warm core ring causes increased phytoplankton levels within the ring itself, on the eastern side. Zooplankton show less depletion in the ring itself, with a somewhat stronger signal in downstream.
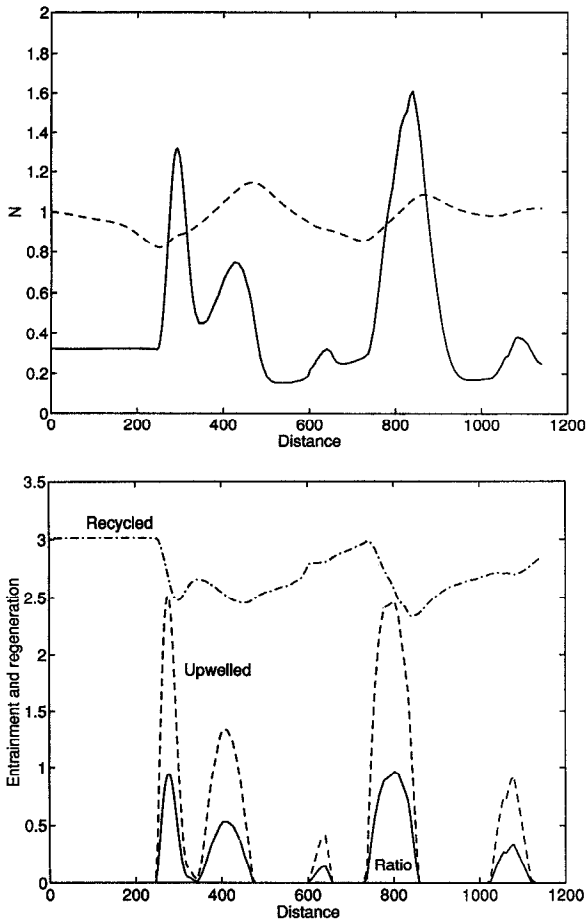
Figure 6.4. (Continued)

7. Summary

We find that the meander-induced entrainment of fluid into the mixed layer has two principal effects: it causes a shift in the average values of the P, Z, and N fields, and it causes variability along the track. In a periodic series of meanders (Figs. 5.3–4), the upwelling and downwelling leads to enhanced phytoplankton and reduced zooplankton and nutrient levels. The phytoplankton peak just downstream of the meander crest while the zooplankton are highest just after the trough. For longer waves, the signals are similar, but with less phase shift and smaller amplitude. The phytoplankton are affected by input of nutrients (dominantly), dilution, and reduced grazing. Dilution is the strongest source of variability for the zooplankton.

The expression for the vertical velocity shows that the stretching is proportional to $c(U_0 - c)$; this is small for both very short and very long waves, peaking at $\lambda = 2\pi R_d / \sqrt{3} =$
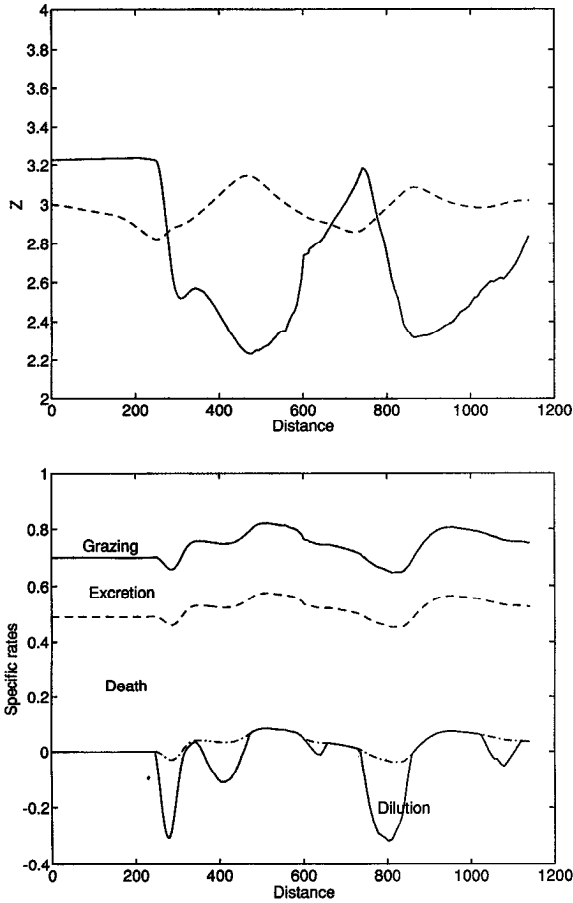
Figure 6.4. (Continued)

108 km. The biological variability is largest for such wavelengths also, as is the shift in the mean (the latter can be calculated analytically for the periodic case). However, the QG 1½ layer model is not expected to be very accurate at such short wavelengths.

The vertical movement of a material surface with concomitant light level changes causes similar variation in phytoplankton levels, but has little impact on the zooplankton. Plankton carried toward the surface along the isopycnal surface below the mixed layer increased in biomass due to increasing light levels. The initial enhancement was approximately proportional to light intensity since nutrients were saturating at this point. The relatively low light levels, however, caused absolute growth rate to be small so that even a large relative increase in growth rate resulted in small changes in mass. The impacts are fairly insensitive to the wavelength.

For plankton in an entraining mixed layer, a single meander produces a high nutrient regime on the northward branch and a slight depression of P as phytoplank-

S on contour
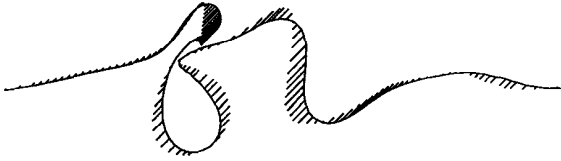
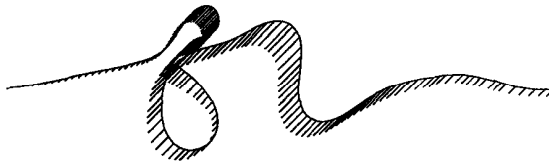Variations in P on contour

Variations in Z on contour

Figure 6.5. Cold ring formation event. Pictures after 3.75 days.

ton are diluted, followed by rapid growth as they take up the new nutrients (Fig. 5.2–4). The zooplankton are diluted strongly and recover slowly as they graze down the phytoplankton.

These calculations certainly suggest that the meander-forced upwelling is a significant influence on the biological populations, especially the shorter scale motions. Although the perturbations to the plankton biomass induced by upwelling are significant, they may be obscured by small scale movements of the strong

cross-stream gradient in biomass from the Slope Water to the Sargasso Sea. Also, because of this gradient, small errors in positioning the material surface representing the PV front may lead to large errors in estimating the along-axis biological variations.

The decrease in zooplankton due to dilution by upwelling is in part due to our simplification that plankton occur only in the mixed layer; without this assumption, one must model the distribution of plankton in the deep layer and invoke a more complex model. Nonetheless, the simple model presented here shows clearly that Gulf Stream meandering can cause significant perturbations to planktonic populations.

REFERENCES

Bower, A. S. 1989. Potential vorticity balances and horizontal divergence along particle trajectories in Gulf Stream meanders east of Cape Hatteras. J. Phys. Oceanogr., *19*, 1669–1681.

—— 1991. A simple kinematic mechanism for mixing fluid parcels across a meandering jet. J. Phys. Oceanogr., *21*, 173–180.

Bower, A. S. and T. Rossby. 1989. Evidence of cross-frontal exchange processes in the Gulf Stream based on isopycnal RAFOS float data. J. Phys. Oceanogr., *19*, 1177–1190.

Dengler, A. T. 1985. Relationship between physical and biological processes at an upwelling front off Peru, 15S. Deep-Sea Res., *32*, 1301–1315.

Flierl and Meacham. 1993. Instabilities and waves on thin jets (in prep).

Franks, P. J. S. 1992. Sink or swim—accumulation of biomass at fronts. Mar. Ecol. Prog. Ser., *82*, 1–12.

Franks, P. J. S., J. S. Wroblewski and G. R. Flierl. 1986. Behavior of a simple plankton model with food-level acclimation by herbivores. Mar. Biol., *91*, 121–129.

Gilham, L. B., J. J. Mika and D. A. Wiesenburg. 1985. Bibliography of research on ocean fronts, 1964–1984. Tech. Note U.S. Navy Ocean Res. Dev. Activity, 58 pp.

Holligan, P. M. 1981. Biological implications of fronts on the northwest European continental shelf. Phil. Trans. R. Soc. Lond. A, *302*, 547–562.

Houghton, R. W. and J. Marra. 1983. Physical/biological structure and exchange across the thermohaline shelf/slope front in the New York Bight. J. Geophys. Res., *88*, 4467–4481.

Huntley, M. and C. Boyd. 1984. Food-limited growth of marine zooplankton. Am. Nat., *124*, 455–478.

Ivlev, V. S. 1955. Experimental Ecology of the Feeding of Fishes. Pischepromizdat, Moscow. 302 p. (Transl. from Russian by D. Scott) New Haven: Yale University Press (1961).

Landry, M. R., R. P. Hassett, V. Fagerness, J. Downs and C. J. Lorenzen. 1984. Effect of food acclimation on assimilation efficiency of *Calanus pacificus*. Limnol. Oceanogr., *29*, 361–364.

Leetma, A. and A. F. Bunker. 1978. Updated charts of the mean annual wind stress, convergence in the Ekman layers and Sverdrup transports in the North Atlantic. J. Mar. Res., *36*, 311–322.

Lewis, M. R., W. G. Harrison, N. S. Oakey, D. Herbert and T. Platt. 1986. Vertical nitrate fluxes in the oligotrophic ocean. Science, *234,* 870–873.

Lutjeharms, J. R. E., N. M. Walters and B. R. Allanson. 1985. "Oceanic frontal systems and biological enhancement," *in* Antarctic Nutrient Cycles and Food Webs, W. R. Siegfried, P. R. Condy, and R. M. Laws, eds., Springer-Verlag, Berlin, 714 pp.

Meacham, S. P. 1991. Meander evolution on piecewise-uniform, quasi-geostrophic jets. J. Phys. Oceanogr., *21,* 1139–1170.

Niiler, P. P. 1977. One-dimensional models of the seasonal thermocline, *in* The Sea, *6,* E. D. Goldberg, I. N. McCave, J. J. O'Brien, J. H. Steele, eds., Wiley-Interscience, New York, 97–115.

Olson, D. B. 1990. BIOSYNOP: Biophysical studies of Gulf Stream meanders. SYN-OPtician, *1(3),* 1–3.

Olson, D. B. and R. H. Backus. 1985. The concentrating of organisms at fronts: a cold-water fish and a warm-core Gulf Stream ring. J. Mar. Res., *43,* 113–137.

Pascual, M. 1993. Diffusion-induced chaos in a spatial predator-prey system. Proc. Roy. Soc. Lond. B, Proc. R. Soc. Lond. B, *251,* 1–7.

Pedlosky, J. 1987. Geophysical Fluid Dynamics. 2nd. ed. Springer-Verlag, New York.

Pratt, L. J. and M. E. Stern. 1986. Dynamics of potential vorticity fronts and eddy detachment. J. Phys. Oceanogr., *16,* 1101–1120.

Price, J. F. 1981. Upper ocean response to a hurricane. J. Phys. Oceanogr., *11,* 153–175.

Richardson, K. 1985. Plankton distribution and activity in the North Sea/Skagerrak-Kattegat frontal area in April 1984. Mar. Ecol. Prog Ser., *26,* 233–244.

Seliger, H. H., K. R. McKinley, W. H. Biggley, R. B. Rivkin and K. R. H. Aspden. 1981. Phytoplankton patchiness and frontal regions. Mar. Biol., *61,* 119–131.

Simpson, J. H., P. B. Tett, M. L. Argote-Espinoza, A. Edwards, K. J. Jones and G. Savidge. 1982. Mixing and phytoplankton growth around an island in a stratified sea. Cont. Shelf Res., *1,* 15–31.

Steele, J. H. 1977. Ecological modeling of the upper layers, *in* Modelling and Prediction of the Upper Layers of the Ocean, E. B. Kraus, ed., Pergamon Press, New York, 325 pp.

Steele, J. H. and E. W. Henderson. 1992. The role of predation in plankton models. J. Plankton Res., *14,* 157–172.

Traganza, E. D., D. G. Redalje and R. W. Garwood. 1987. Chemical flux, mixed layer entrainment and phytoplankton blooms at upwelling fronts in the California coastal zone. Cont. Shelf Res., *7,* 89–105.

Wroblewski, J. S., J. L. Sarmiento and G. R. Flierl. 1988. An ocean basin scale model of plankton dynamics in the North Atlantic. 1. Solutions for the climatological oceanographic conditions in May. Global Biogeochem. Cycles, *2,* 199–218.

Yoder, J. A., L. P. Atkinson, T. N. Lee, H. H. Kim and C. R. McClain. 1981. Role of Gulf Stream frontal eddies in forming phytoplankton patches on the outer southeastern shelf. Limnol. Oceanogr., *26,* 1103–1110.